Joint seismic traveltime and TEM inversion for near surface imaging

Jide Nosakare Ogunbo, Jie Zhang, GeoTomo LLC*

Summary

For a reliable interpretation of the subsurface structure, the joint geophysical inversion approach is becoming a viable tool. Seismic and EM methods are quite complementary because they measure different physical properties. The high expenditure for field operation of Transient EM (TEM) data acquired over 2D and 3D survey geometry have usually limited acquisition of TEM data to single soundings interpreted as a 1D subsurface resistivity. The minimum spatial dimension for joint inversion with structural (cross-gradient) constraints is 2D. To take advantage of the gains from joint inversion we develop a method for pseudo-2D TEM data inversion using a 1D forward code. We combine the pseudo-2D TEM inversion and 2D traveltime inversion for joint inversion with cross-gradient constraints between seismic slowness and electrical resistivity. We demonstrate that joint inversion is able to reconstruct seismic velocities and resistivity distribution with consistent geology better than individual seismic or resistivity inversions.

Introduction

Joint geophysical inversion of multiple data sets has recently become an interpretation approach for defining subsurface geology (Gallardo and Meju, 2003; Gallardo and Meju, 2004; Abubakar et al., 2012). This is justified because rock properties are not limited to a single physical property e.g. velocity, conductivity, magnetic susceptibility. Joint inversion of multiple model parameters with structural or petrophysical correlations should display consistent geology (Zhang and Morgan, 1996).

There are two classes of constraints that can be applied in a joint geophysical inversion: petrophysical and structural constraints (Gallardo and Meju, 2004; Abubakar et al., 2012). Because seismic velocity and electrical resistivity are not directly linked, Zhang and Morgan (1996) imposed structural constraints for the joint reconstruction of seismic velocity and electrical resistivity. Gallardo and Meju (2003) and Gallardo and Meju (2004) describe how to apply structural constraints by cross-gradient in a joint inversion. They successfully applied their concept on the joint 2D inversion of DC resistivity and seismic traveltime data. Abubakar et al., (2012) applied both petrophysical and structural constraints for the joint inversion of controlled-source electromagnetic (CSEM) data with surface seismic full-waveform data.

Our study presents joint inversion of TEM and seismic traveltime data. Both seismic and EM methods are complementary: low-velocity zones which are difficult to image by seismic method alone but may have a dominant electrical conductivity anomaly (Zhang and Morgan, 1996). Conventionally, joint inversion is done by a combination of multiple data on the same spatial dimension (e.g.: 2D DC resistivity and 2D traveltime inversion, Gallardo and Meju, 2004). However, in this study we demonstrate the feasibility of doing joint inversion using data acquired in different spatial dimensions. We shall perform pseudo-2D TEM data inversion using a 1D forward code and 2D Tikhonov regularization of the resistivity model. Then we perform the joint inversion using cross-gradient constraints by a conjugate gradient (CG) method.

Pseudo-2D TEM inversion

On one hand, interpretation of 1D TEM data is inherently non-unique (Patra and Mallick, 1980; Spies and Frischknecht, 1991). On the other hand, the computational overhead of imaging real 2D and 3D TEM data is humongous (Schultz and Ruppel, 2005; Schamper et al., 2012). Therefore, to be cost-effective, and more reliable in interpretation, Schultz and Ruppel (2005) performed a pseudo-2D inversion of multiple 1D EM data. This concept was used by Auken and Christiansen (2004) for resistivity inversion. Schamper et al., (2012) used the same idea for the inversion of multifrequency and multicomponent ground-based electromagnetic induction data.

We apply this concept to solve a 2D TEM inversion problem from combined multiple 1D forward models. The objective function is a regularized least-squares:

$$\emptyset(\mathbf{m_r}) = \|\mathbf{d_r} - \mathbf{G}(\mathbf{m_r})\|^2 + \boldsymbol{\tau_r}\|\mathbf{L}\mathbf{m_r}\|^2 , \qquad (1)$$

where $\mathbf{d_r}$ is the data vector, $\mathbf{G}(\mathbf{m_r})$ is the computed data vector using natural logarithm resistivity model parameter $\mathbf{m_r}$, $\mathbf{L}$ is the roughening matrix, and $\boldsymbol{\tau_r}$ is the smoothing trade-off parameter. After equating the derivative of Equation (1) with respect to the model parameter to zero, we have:

$$\left(\mathbf{A_r^T C_{d_r}^{-1} A_r} + \boldsymbol{\tau_r} \mathbf{L^T L} + \boldsymbol{\epsilon_r^k} \boldsymbol{I}\right)\Delta \mathbf{m_r^k} = \mathbf{A_r^T C_{d_r}^{-1}} \Delta \mathbf{d_r} - \boldsymbol{\tau_r} \mathbf{L^T L m_r^k} , \qquad (2)$$

where $\mathbf{A_r}$ is the sensitivity matrix, $\Delta \mathbf{d_r}$ is the data difference vector, $\mathbf{C_{d_r}}$ is the data covariance matrix

DOI http://dx.doi.org/10.1190/segam2014-1056.1

(Tarantola, 2005), $\mathbf{m_r^k}$ is the model parameter at k-th iteration, $\Delta\mathbf{m_r^k}$ is the model update at k-th iteration, $\epsilon_\mathbf{r}^\mathbf{k}\boldsymbol{I}$ is an iteration variable damping term (Zhang and Toksöz, 1998). Equation (2) can be inverted to find $\Delta\mathbf{m_r^k}$ using a CG inversion method. The model parameter at (k+1)-th iteration is then simply calculated as:

$$\mathbf{m_r^{k+1}} = \mathbf{m_r^k} + \Delta\mathbf{m_r^k}, \quad \mathbf{k} = \mathbf{1}, \mathbf{2}, \mathbf{3}, \ldots, \mathbf{N}. \tag{3}$$

For the forward modeling computation of circular central-loop TEM data we use the 1D formulation by Ward and Hohmann (1987). Each of the multiple resistivity data vectors and the computed data vectors are 1D. The pseudo-2D TEM is made possible by the use of a 2D roughening matrix, $\mathbf{L}$. This eventually results into a pseudo-2D sensitivity matrix, $\mathbf{A_r}$. Because $\mathbf{L}$ can exist in any dimension (1D, 2D or 3D), it is trivial to extend this concept to pseudo-3D from either 1D or 2D combinations.

Structurally constrained joint inversion

With a cross-gradient as a structural constraint, $\boldsymbol{t}$ (Gallardo and Meju, 2003; Gallardo and Meju, 2004), the joint inversion objective function we seek to minimize is given as:

$$\emptyset(\mathbf{m_r}, \mathbf{m_s}) = \boldsymbol{\omega_r}\|\mathbf{d_r} - \mathbf{G}(\mathbf{m_r})\|^2 + \boldsymbol{\omega_s}\|\mathbf{d_s} - \mathbf{G}(\mathbf{m_s})\|^2 + \boldsymbol{\tau_r}\|\mathbf{L}\mathbf{m_r}\|^2 + \boldsymbol{\tau_s}\|\mathbf{L}\mathbf{m_s}\|^2 + \boldsymbol{\lambda}\|\boldsymbol{t}\|^2. \tag{4}$$

All variables retain their previous definitions but the ones with subscript **s** correspond to seismic method; $\boldsymbol{\omega_r}$ **and** $\boldsymbol{\omega_s}$ are the resistivity and seismic data misfit scaling factors where $\boldsymbol{\omega_r} = \mathbf{1} - \boldsymbol{\omega_s}$; $\mathbf{G}(\mathbf{m_s})$ is the first-arrival time data (computed using the 2D traveltime code of Zhang and Toksöz, (1998)). The cross-gradient constraint $\boldsymbol{t}$ is given as (Gallardo and Meju, 2003; Gallardo and Meju, 2004):

$$\boldsymbol{t}(\mathbf{m_r}, \mathbf{m_s}) \cong \boldsymbol{t_0}(\mathbf{m_{0r}}, \mathbf{m_{0s}}) + \mathbf{B}\begin{pmatrix}\mathbf{m_r} - \mathbf{m_{0r}} \\ \mathbf{m_s} - \mathbf{m_{0s}}\end{pmatrix}, \tag{5}$$

$$\boldsymbol{t_0}(\mathbf{m_{0r}}, \mathbf{m_{0s}}) = \boldsymbol{\nabla}\mathbf{m_{0r}}(\mathbf{x}, \mathbf{y}) \times \boldsymbol{\nabla}\mathbf{m_{0s}}(\mathbf{x}, \mathbf{y}). \tag{6}$$

It should be noted that cross product, in Equation (6), for 1D is zero. Thus a cross-gradient constraint cannot be imposed while jointly inverting 1D velocity and resistivity structures. This is one of the reasons for doing a pseudo-2D TEM inversion from multiple 1D TEM forward models.

$\mathbf{B}$ is the partial derivative of $\boldsymbol{t}$ with respect to the model parameters, $\mathbf{m_{0r}}$ and $\mathbf{m_{0s}}$ are the initial resistivity and velocity models respectively; $\boldsymbol{\lambda}=\begin{pmatrix}\boldsymbol{\lambda_r} \\ \boldsymbol{\lambda_s}\end{pmatrix}$ is the scaling factor for the cross-gradient constraints. Details about the evaluation of Equations (5) and (6) are given by Gallardo and Meju (2003). After substituting Equations (5) and (6) into Equation (4) and equating its derivative with respect to the model parameters to zero, the objective function can be minimized, giving:

$$\begin{pmatrix}\boldsymbol{\omega_r}\mathbf{A_r^T}\mathbf{C_{d_r}^{-1}}\mathbf{A_r} + \boldsymbol{\tau_r}\mathbf{L^T}\mathbf{L} + \epsilon_\mathbf{r}^\mathbf{k}\boldsymbol{I} & \mathbf{0} \\ \mathbf{0} & \boldsymbol{\omega_s}\mathbf{A_s^T}\mathbf{C_{d_s}^{-1}}\mathbf{A_s} + \boldsymbol{\tau_s}\mathbf{L^T}\mathbf{L} + \epsilon_\mathbf{s}^\mathbf{k}\boldsymbol{I}\end{pmatrix} \times \begin{pmatrix}\Delta\mathbf{m_r} \\ \Delta\mathbf{m_s}\end{pmatrix} + \boldsymbol{\lambda}\mathbf{B^T}\mathbf{B}\begin{pmatrix}\Delta\mathbf{m_r} \\ \Delta\mathbf{m_s}\end{pmatrix} = \begin{pmatrix}\boldsymbol{\omega_r}\mathbf{A_r^T}\mathbf{C_{d_r}^{-1}}\Delta\mathbf{d_r} - \boldsymbol{\tau_r}\mathbf{L^T}\mathbf{L}\mathbf{m_{0r}^k} \\ \boldsymbol{\omega_s}\mathbf{A_s^T}\mathbf{C_{d_s}^{-1}}\Delta\mathbf{d_s} - \boldsymbol{\tau_s}\mathbf{L^T}\mathbf{L}\mathbf{m_{0s}^k}\end{pmatrix} - \boldsymbol{\lambda}\mathbf{B^T}\boldsymbol{t_0}. \tag{7}$$

For the (k+1)-th iteration, the model parameter becomes

$$\begin{pmatrix}\mathbf{m_r^{k+1}} \\ \mathbf{m_s^{k+1}}\end{pmatrix} = \begin{pmatrix}\mathbf{m_{0r}^k} + \Delta\mathbf{m_r^k} \\ \mathbf{m_{0s}^k} + \Delta\mathbf{m_s^k}\end{pmatrix}, \quad \mathbf{k} = \mathbf{1}, \mathbf{2}, \mathbf{3}, \ldots, \mathbf{N}. \tag{8}$$

The model update $\begin{pmatrix}\Delta\mathbf{m_r} \\ \Delta\mathbf{m_s}\end{pmatrix}$ is found by the CG method. The CG method is the preferred inversion method because quite a large number of model parameters are involved in 2D tomography imaging (Rawlinson and Sambridge, 2003), even more for 3D imaging and joint inversion. Because the sensitivity matrix storage (of Equation 7) can be avoided (Zhang and Toksöz, 1998), the CG algorithm is computationally affordable (Sadiku, 2009).

Synthetic experiments

We demonstrate the joint inversion concept described in the previous sections using both a known velocity and a known resistivity model with similar structure. The true models are close to those in Gallardo and Meju (2004) with two rectangular blocks embedded in a half space. The properties of the models are found in Table 1.

Figure 1 shows the true velocity and resistivity models. The horizontal extent of these models is 295m and the total depth of investigation is set at 60m. The grid size is 5m and is uniform in both horizontal and vertical directions. This uniform discretization amounts to generating 59 square central-loop 1D TEM data points, each of which is produced with transmitter area of 400m^2 and unit receiver area of 1m^2. Each of the transient voltage has 20 time samples logarithmically spaced between 0.1ms and 10.0ms.

The first-arrival traveltimes are computed using the 2D raytracing code of Zhang and Toksöz (1998) with 90 shots and 94 receivers positioned on the surface. The seismic ray coverage (Figure 2) shows which areas in the model space

DOI http://dx.doi.org/10.1190/segam2014-1056.1

are well conditioned by the data coverage. Only the top of the rectangular blocks will be reconstructed if only seismic refraction method is used to image this model, because no critically refracted rays are generated below these blocks.

	Resistivity model (Ωm)	Velocity model (m/s)
Half space	100	1000
Left box	10	2000
Right box	1000	2000

Table 1: Resistivity and Velocity models for joint inversion

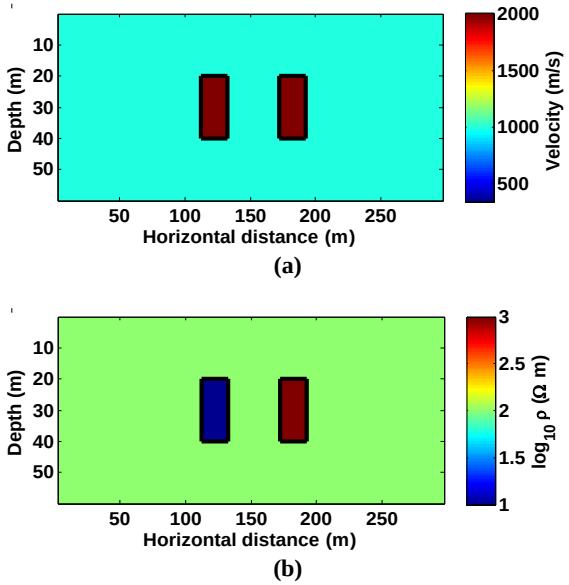

Figure 1: (a) True velocity model and (b) true resistivity model with same geologic structures (rectangular blocks). The properties of the blocks are in Table 1.

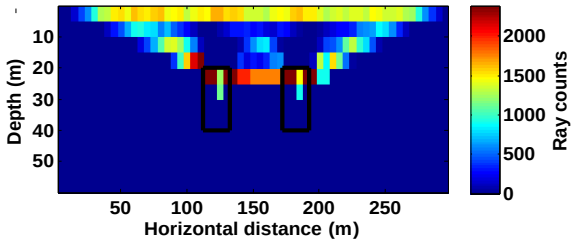

Figure 2: Ray counts generated from velocity model in Figure 1a. High counts indicate the model space that is well conditioned by data.

Results and discussion

Both individual and joint inversion results are compared in this section. Figure 3 shows the model resulting from individual inversions of velocity and resistivity (after 20 iterations in the CG scheme). As expected because of the poor ray coverage (Figure 2), the rectangular blocks are not reconstructed by the velocity inversion (see Figure 3a). The conductive rectangular block is well imaged by resistivity inversion (Figure 3b), but the resistive block is only faintly outlined. This is because the TEM method relies on induction and is more sensitive to high conductivity.

For the joint inversion, trials are made before choosing the ratio of the cross-gradient parameters ($\boldsymbol{\lambda_r}$, $\boldsymbol{\lambda_s}$). Because $\boldsymbol{\tau_r}$, $\boldsymbol{\tau_s}$, $\boldsymbol{\lambda_r}$ and $\boldsymbol{\lambda_s}$ are all factors that influence structures, we aim to set the roughening trade-off parameters ($\boldsymbol{\tau_r}$, $\boldsymbol{\tau_s}$,) in such a way that they do not overshadow, suppress, or undo the effect of the cross-gradient constraints ($\boldsymbol{\lambda_r}$, $\boldsymbol{\lambda_s}$) during the joint inversion process. Figure 4 shows the results from joint inversion of velocity and resistivity models (after 20 iterations). Although, the rectangular blocks of the velocity model are not illuminated by seismic refractions (due to limited ray path coverage), at the early iteration of the CG scheme the resistivity structure imposes a structural constraint on the jointly inverted velocity model. While the CG scheme iterates, the structural constraint contributions are from both the velocity and resistivity models. This ultimately enhances the resolution of the more resistive structure and eventually reduces smearing in this image.

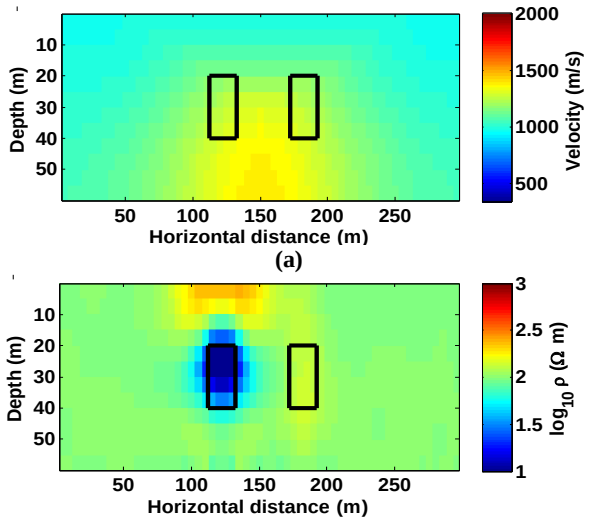

Figure 3: (a) velocity model result (b) resistivity models result from separate inversion

DOI http://dx.doi.org/10.1190/segam2014-1056.1

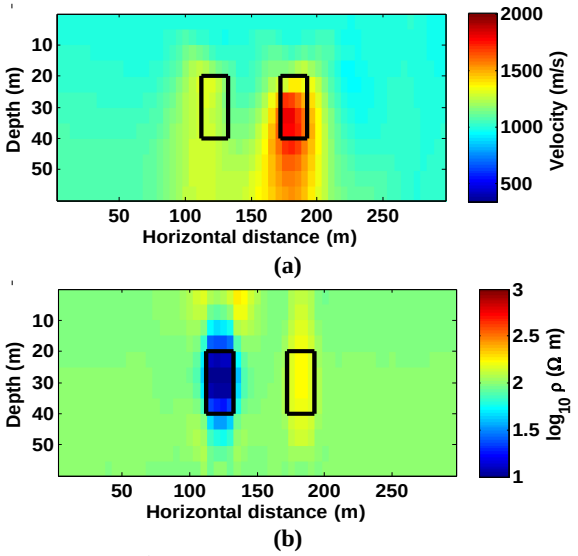

Figure 4: Result from joint inversion with structural constraints, (a) velocity model, (b) resistivity model.

Figure 5 displays comparison between seismic traveltime data computed from the true model and inverted model for both separate and joint inversion. The root mean square error of the data computed from joint inversion is 0.68802ms while that of the data computed from separate inversion is 0.71409ms.

The difference between the computed data from true resistivity model and data from the separate and joint inverted models are compared in Figure 6. Six of the 59 data points, starting from 25m horizontal distance in steps 35m apart, are displayed in Figure 6. Figures 6a, b, e and f represent a section of the model far from the rectangular blocks while Figures 6c and d, show plots from a section of the model in the vicinity of the rectangular blocks. From these figures, it is observed that the joint inversion results have smaller deviation than the separate inversion results.

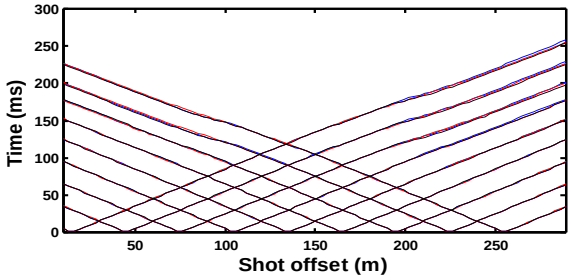

Figure 5: Comparison of data from true velocity model (blue) with data from separate (red) and joint inversion (black).

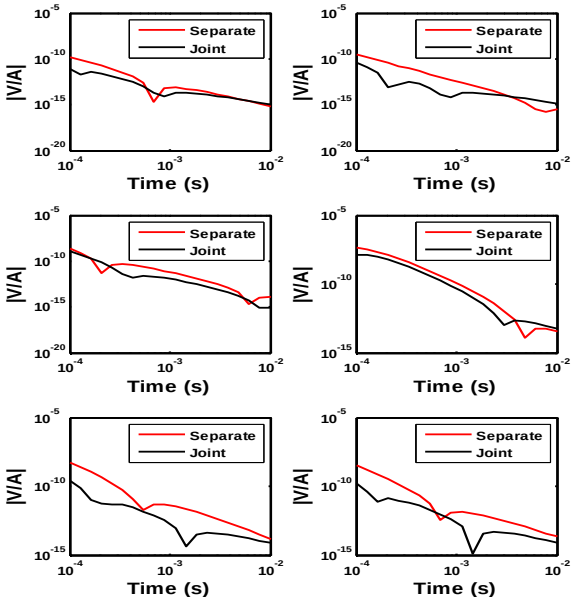

Figure 6: Absolute difference between data computed from true resistivity model and data from separate and joint inversion.

Conclusions

We develop a joint inversion of pseudo-2D TEM and 2D traveltime data with cross-gradient constraints.

Structurally constrained joint inversion could only be done on models with at least two spatial dimensions, but for computational reasons TEM data are mostly acquired on 1D geometry. This necessitates the creation of pseudo-2D TEM geometry using 1D TEM forward code. We then jointly invert these pseudo-2D TEM and 2D traveltime data. We present a test with a synthetic model test in which the structures are inherently invisible to seismic refraction tomography, but electromagnetically visible. Thus, the joint inversion ensures that the electrical conductivity measurements impose a similar structure on velocity structure. Therefore, the final jointly inverted near surface models are of consistent geology.

Acknowledgments

We thank Guy Marquis at Shell for helpful discussion on the research project, and for his comments and suggestions to improve the manuscript. We appreciate the project sponsorship from Shell.

DOI http://dx.doi.org/10.1190/segam2014-1056.1

http://dx.doi.org/10.1190/segam2014-1056.1

EDITED REFERENCES

Note: This reference list is a copy-edited version of the reference list submitted by the author. Reference lists for the 2014 SEG Technical Program Expanded Abstracts have been copy edited so that references provided with the online metadata for each paper will achieve a high degree of linking to cited sources that appear on the Web.

REFERENCES

Abubakar, A., G. Gao, T. M. Habashy, and J. Liu, 2012, Joint inversion approaches for geophysical electromagnetic and elastic full-waveform data: Inverse Problems, **28**, doi:10.1088/0266-5611/28/5/055016.

Auken, E., and A. V. Christiansen, 2004, Layered and laterally constrained 2D inversion of resistivity data: Geophysics, **69**, 752–761, http://dx.doi.org/10.1190/1.1759461.

Gallardo, L. A., and M. A. Meju, 2003, Characterization of heterogeneous near-surface materials by joint 2D inversion of dc resistivity and seismic data: Geophysical Research Letters, **30**, no. 13, 1658, http://dx.doi.org/10.1029/2003GL017370.

Gallardo, L. A., and M. A. Meju, 2004, Joint two-dimensional DC resistivity and seismic traveltime inversion with cross-gradients constraints: Journal of Geophysical Research, **109**, B3, B03311, http://dx.doi.org/10.1029/2003JB002716.

Patra, H. P., and K. Mallick, 1980, Geosounding principles, 2: Methods in geochemistry and geophysics: Elsevier.

Rawlinson, N., and M. Sambridge, 2003, Advances in geophysics, Seismic traveltime tomography of the crust and lithosphere: Academic Press.

Sadiku, M., 2009, Numerical techniques in electromagnetic with Matlab, 3rd ed.: CRC.

Schamper, C., F. Rejiba, and G. Roger, 2012, 1D single-site and laterally constrained inversion of multifrequency and multicomponent ground-based electromagnetic induction data — Application to the investigation of a near-surface clayey overburden: Geophysics, **77**, no. 4, WB19–WB35, http://dx.doi.org/10.1190/GEO2011-0358.1.

Schultz, G., and C. Ruppel, 2005, Inversion of inductive electromagnetic data in highly conductive terrains: Geophysics, **70**, no. 1, G16–G28, http://dx.doi.org/10.1190/1.1852775.

Spies, B. R., and F. C. Frischknecht, 1987, Electromagnetic methods in applied geophysics: SEG.

Tarantola, A., 2005, Inverse problem theory and methods for model parameter estimation: SIAM.

Ward, S. H., and G. W. Hohmann, 1987, Electromagnetic theory for geophysical applications, *in* M. N. Nabighian, ed., Electromagnetic methods in applied geophysics: SEG, 131–311.

Zhang, J., and F. D. Morgan, 1996, Joint seismic and electrical tomography: Presented at Symposium on Applications of Geophysics to Engineering and Environmental Problems, EEGS.

Zhang, J., and M. N. Toksöz, 1998, Nonlinear refraction traveltime tomography: Geophysics, **63**, 1726–1737, http://dx.doi.org/10.1190/1.1444468.